

EVIDENCE OF ROTATION IN FLAME-STRUCTURE PEARLS FROM BIVALVES OF THE TRIDACNIDAE FAMILY

Jean-Pierre Gauthier, Jacques Fereire, and Thanh Nhan Bui

Thirty-seven pearls originating from bivalves of the Tridacnidae family were analyzed to determine their gemological properties and to characterize the optical features of their distinctive flame structure, terminating at the apex and base with patterns like those of blade impellers. All but two of the samples exhibited cylindrical symmetry around a fixed axis, suggesting a rotating movement during growth, as with numerous pearls from *Pinctada margaritifera*. One quite unusual feature, which is difficult to detect and to our knowledge has never before been described, consisted of spiral patterns at the apex and base of the pearl, and one of these patterns suggested the possibility of rotation. Other details that supported the conclusion of rotation during growth included comets associated with spot defects and pseudo-chatoyancy that appeared shifted to one side.

A number of marine organisms produce aragonitic pearls with microstructures different from the nacreous layers generally observed in various bivalves such as the saltwater *Pinctada* and *Pteria* species or the freshwater *Hyriopsis* species. These non-nacreous pearls have a microstructure consisting of crossed aragonitic lamellae (Jiao et al., 2016; Agbaje et al., 2017). These specimens possess a “flame” structure that can be observed under the microscope, with a large base and an elongated tail terminating in one or more tips. They sometimes display an optical phenomenon resembling chatoyancy.

Some marine gastropods produce concretions with a flame structure. One of the most famous is the pink conch “pearl” from *Strombus gigas*, a gastropod that has been fished for its flesh and concretions, and these concretions have even been cultured (Davis, 2000; Davis and Shawl, 2005; Segura and Fritsch, 2015). In addition to salmon pink, these concretions can display white, brown, golden, or yellow hues. The history and gemology of the conch pearl have been reported by Fritsch and Misiorowski (1987) and Federman and Bari (2007). Similar to these are *Lambis*

truncata pink pearls (Bari and Lam, 2009, p. 68). Less well documented are flame-structure pearls from the *Melo* species (Htun et al., 2006), with a color ranging from orange to brown and in light, vivid, or dark hues

In Brief

- Like nacreous pearls from various bivalves, non-nacreous pearls from the Tridacnidae family may display an axial symmetry.
- Distinct flames develop in a crisscross pattern around the rotation axis and converge toward the poles as blade impellers.
- These figures, in addition to other features such as polar spirals, comets, and pseudo-chatoyancy, are evidence of the rotation during formation in flame-structure pearls.

(Scarratt, 1999; Htun et al., 2006). Even rarer in the literature are the flame-structure pearls from *Cassis cornuta* (Bari and Lam, 2009, pp. 73–75) and *Pleuroploca gigantea* (Koivula et al., 1994).

The flame structure is encountered in some bivalves. Except for rare cases of species from the *Spondylus* genus (Ho and Zhou, 2014; Homkrajae, 2016a,b), these belong to the Tridacnidae (also referred to as Tridacninae) family, which contains two genera, *Tridacna* and *Hippopus* (figure 1). *Tridacna gigas* has

See end of article for About the Authors and Acknowledgments.

GEMS & GEMOLOGY, Vol. 55, No. 2, pp. 216–228,

<http://dx.doi.org/10.5741/GEMS.55.2.216>

© 2019 Gemological Institute of America

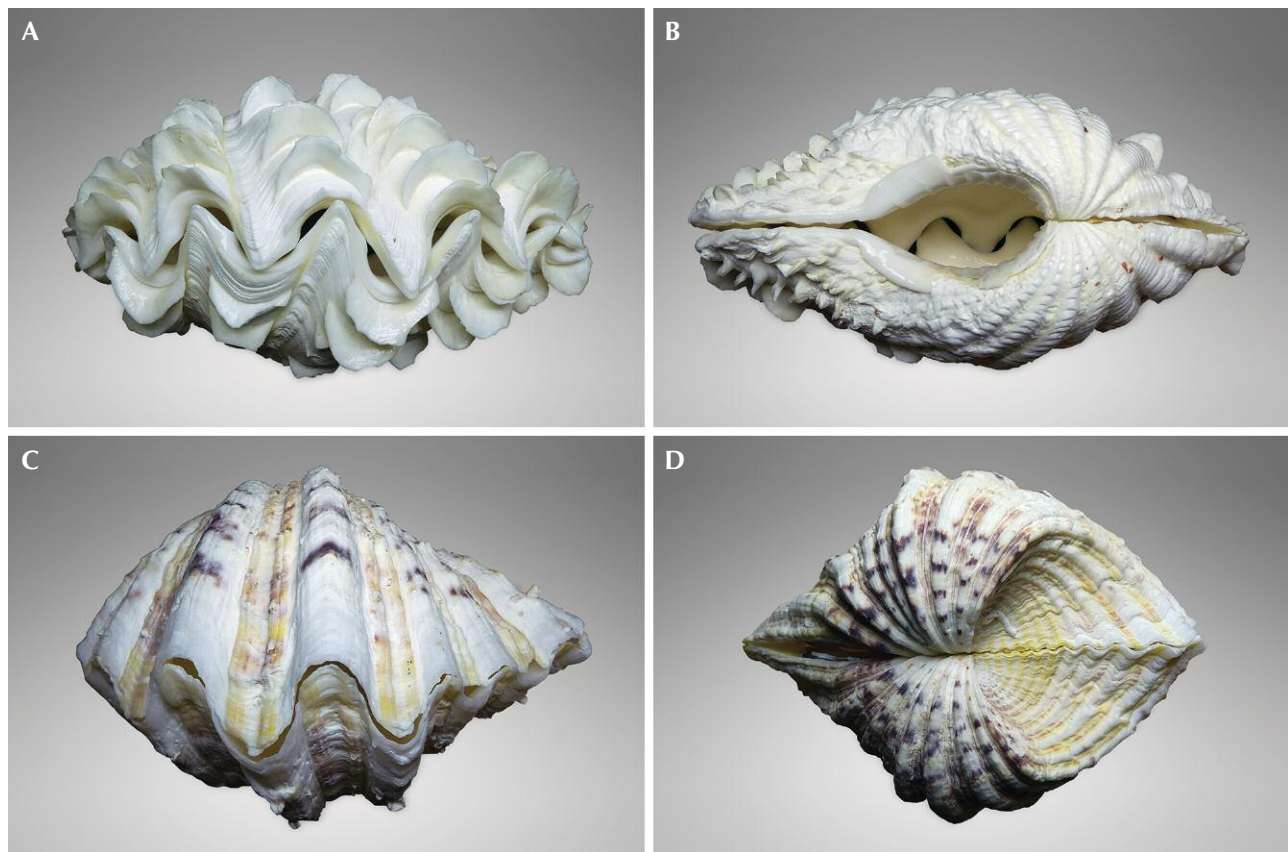


Figure 1. Examples of shells (front and back side) from both *Tridacnidae* genera: *Tridacna maxima* (A and B, shell length 18.5 cm) and *Hippopus* (C and D, shell length 19 cm). Photos by T.N. Bui.

yielded very large non-nacreous concretions, such as the approximately 6.37 kg “Pearl of Allah” (Strack, 2006) and the “Pearl of Elias.” Both are blister pearls: The former has been cut from the shell, and the latter is still attached to its shell. But the species has also produced beautiful flame-structure pearls weighing several tens of carats. The pearls from *Hippopus* or other *Tridacna* species are significantly smaller, weighing only a few carats. From these species we obtained an assortment of 37 pearls, mainly from *Tridacna gigas*, *Tridacna maxima*, and *Tridacna squamosa*, and possibly from *Hippopus hippopus* (figure 2).

The largest species in the *Tridacnidae* family, the giant clam (*Tridacna gigas*), possesses a shell that can reach 1.5 m in length and produces non-nacreous pearls of significant size (Bidwell et al., 2011). While the size of most naturally grown pearls is in the range of one to several centimeters, the previously mentioned “Pearl of Allah” measures 23 cm in length. Such pearls, described as chalky concretions, are of poor quality and usually do not present a visible flame structure (Bari and Lam, 2009).

Other species from the family (*Tridacna derasa*, *Tridacna maxima*, *Tridacna squamosa*, and *Hippopus hippopus*) have shells that only measure up to tens of centimeters in length, and they produce smaller concretions and pearls. These present a flame structure that is visible to the unaided eye.

All species of the *Tridacnidae* family are protected under the European Union (Council of the European Union, 1997), the Convention on International Trade in Endangered Species of Wild Flora and Fauna (CITES), and the International Union for Conservation of Nature (IUCN). However, *Tridacna maxima* is bred in ponds for the aquarium market. It is also cultivated at the French Research Institute for Exploitation of the Sea (IFREMER) in Tahiti for research purposes (Garen, 2003). Unlike conch pearls, for which cultivation has been reported (Acosta-Salmón and Davis, 2007), to the best of our knowledge no pearls have been harvested from bivalves of the *Tridacnidae* family.

Geographic distribution varies within the *Tridacnidae* family. For all species combined, the popula-

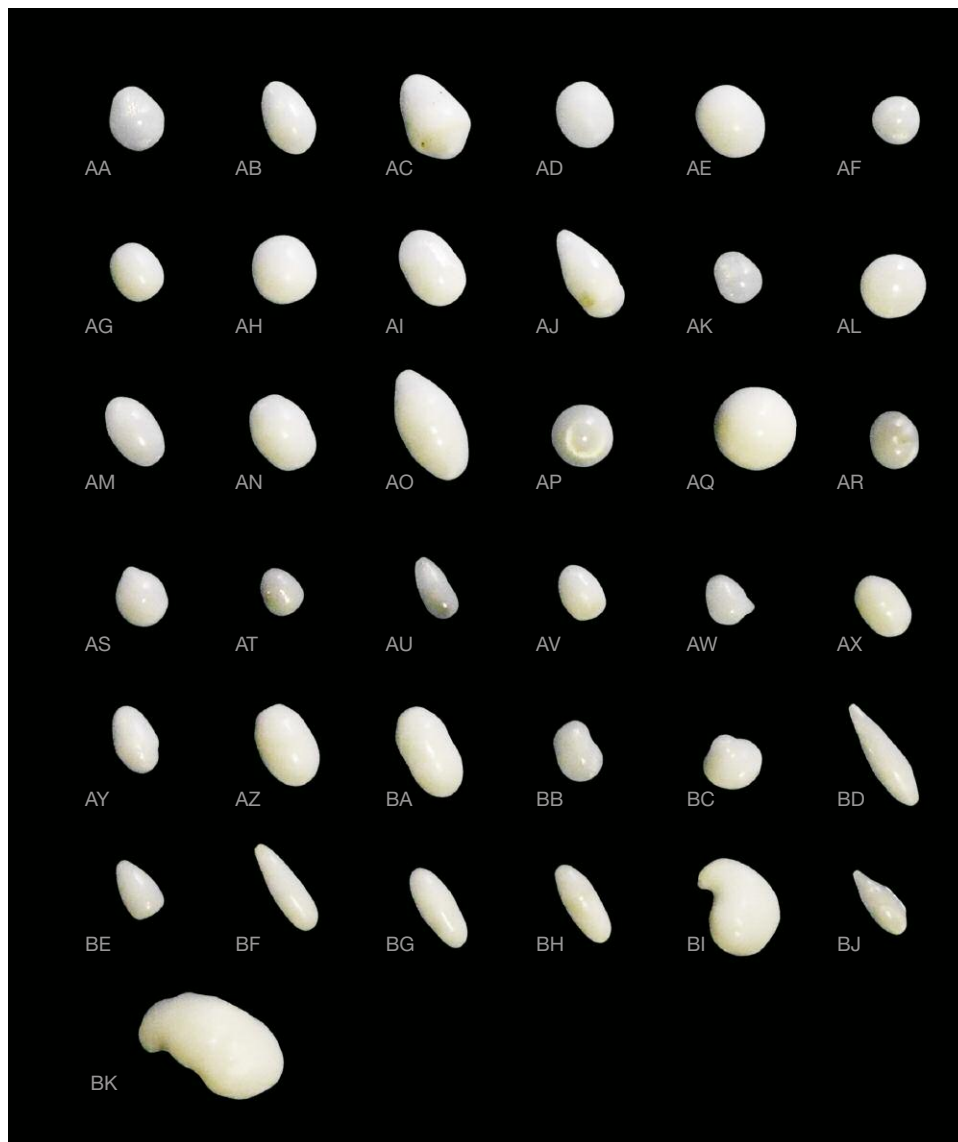


Figure 2. The 37 pearls from this study, ranging from 1.67 to 20.28 ct. Photo by J.-P. Gauthier.

tion of this bivalve extends from the seas south of China to the north of Australia and from Myanmar to Fiji. *Tridacna squamosa* and *Tridacna maxima* are distributed across the Indian Ocean to the east coast of Africa and far into the Pacific Ocean (Copland and Lucas, 1988; Hui, 2012).

Other species such as *Tridacna crocea*, *Tridacna rosewateri*, *Tridacna tevoroa*, and *Hippopus porcellanus* are probably also able to produce pearls, despite not having been mentioned by merchants of natural pearls or in the gemological literature. This may be explained by the small size of their shells (*Tridacna crocea*), their limited geographic distribution, and the absence of known specimens.

Our set of 37 pearls from the Tridacnidae family originated from Indonesia. They were purchased

from traders who collected them from several islands. These traders had taught locals to check for pearls inside the mollusk before cooking the meat. Most of the time the exact origin of the *Tridacna* species was not documented, but systematic tracking was requested for recent acquisitions.

This article will describe the main gemological characteristics of these pearls and detail the features visible to the unaided eye or under the microscope. We will also discuss the characteristics that strongly suggest a rotation of the forming pearl inside the mollusk, similar to that demonstrated in pearls from *Pinctada margaritifera* (Gueguen et al., 2015). Pearl rotation is a frequent phenomenon that occurs around several random axes for round pearls or around one fixed axis for pearls that display an axial

symmetry (see Gauthier et al., 2014, 2015, 2018). In fact, these authors observed that the circles found in Tahitian pearls are induced by spot defects, which are the emergence of tubular cavities perpendicular to the pearl surface and similar to chimney-like structures, sometimes opening out on the surface. The circles form as an asymmetrical comet-shaped structure, which allows us to infer the rotation direction of the pearl.

GEMOLOGICAL DATA

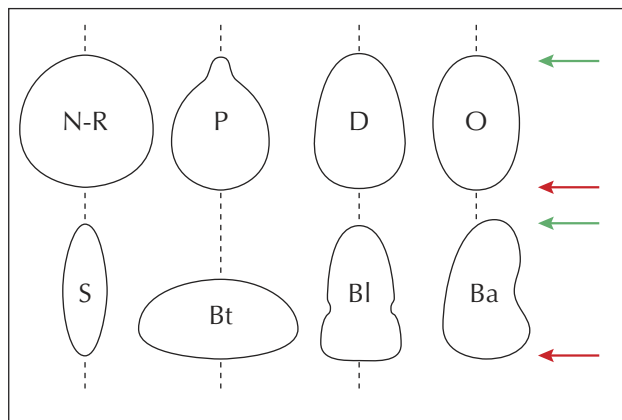
Table 1 presents data on all 37 pearl samples from the Tridacnidae family.

Shape and Symmetry. Figure 3 illustrates the forms observed in the 37 samples from this study. Most of these pearls, labeled in figure 2, exhibited an axial symmetry, except for two baroque pearls with a bean shape (BI and BK). Some presented a classical symmetry in pear or drop shapes. There were no round pearls but two near-round (AF and AQ). Quite a few had an oval shape (AD, AE, AG, AM, AN, AR, AX, AZ, BA, and BB) and some a spindle (AO, BD, BF, BG, BH, and BJ) or bullet shape (AJ, AV, AW, AY, and BE).

For the sake of clarity, the photo labels will refer to the:

1. apex (a): the sharpest upper pole (for example, "AG-a" on the far right of figure 4)
2. base (b): the more rounded lower pole for axially symmetric pearls
3. side (s): the lateral surfaces of the pearls

Figure 3. The main shapes observed in pearls from the Tridacnidae family. N-R = near-round, P = pear, D = drop, O = oval, S = spindle, Bt = button, Bl = bullet, Ba = baroque. The green arrows point to the apex, the red arrows to the base.



For the oval-shaped pearls, the choice of apex and base is obviously arbitrary.

Dimensions and Weight. With previously reported flame-structure pearls, dimensions have varied from a few millimeters to several centimeters and weights reaching tens of carats. These were reported for *Tridacna gigas* (Bidwell et al., 2011) and different *Melo* species (Scarratt, 1999) or other gastropods (Hyatt, 2008; Chang and Hyatt, 2011). The pearls in the present study, from *Tridacna gigas*, *T. maxima*, and *T. squamosa*, as well as *Hippopus* species, are smaller, measuring 16 mm or less and weighing between 1.67 and 20.28 ct.

Density. Each sample's density was obtained using a Sartorius CP323S scale and given as the average of three measurements. Values fell mostly between 2.70 and 2.86, comparable to aragonitic conch pearls (Fritsch and Misiorowski, 1987). In a few cases where the recorded value was low, ranging from 2.31 to 2.63, we assume the existence of an internal cavity, particularly in two samples (AC and AR) that contained a pit, which was also demonstrated in an X-ray radiograph by Singbamroong et al. (2015).







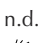










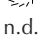









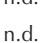

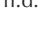





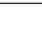





Refractive Index. As the pearls did not have flat surfaces, we had to estimate the refractive indices using the distant vision or spot refractive index method. Most of the samples were elongated and had to be laid down on their sides in the refractometer. Measured RI values ranged from 1.620 to 1.655. Our range of values lies in the mid to high range of the refractive index of aragonite. Among the less-pointed pearls, we tried a single measurement along the pole axis. The measured indices were often weak but did not systematically yield a value close to the lowest index.

Crystallochemical Nature of Pearl AC. X-ray diffraction analysis conducted on sample AC revealed peaks typical of aragonite and no component attributable to calcite. This is consistent with the aragonitic composition of Tridacnidae shells (Dauphin and Denis, 2000; Gannon et al., 2017).

Short-Wave and Long-Wave UV. No reaction to ultraviolet radiation was observed.

Color. Thirty-three of the pearl samples presented a white bodycolor with no additional hues. Four pearls (see figure 15) had a slightly yellowish pit-type defect.

TABLE 1. Gemological data for the set of 37 pearls from the Tridacnidae family.

Sample no.	Symmetry	Shape	Diameter (mm)	Height (mm)	Weight (ct)	Density	RI (⊥)	RI ()	Flame + Ψ_{CE} ^a	Spiral and/or blade impeller ^b (figure 13)	
										Apex	Base
AA	Axial	Pear	9.71	8.36	4.68	2.80	1.64	1.67	Flame		
AB	Axial	Drop	11.90	7.66	4.73	2.79	1.63	—	Flame	n.d. ^c	n.d.
AC	Axial	Pear	9.71	14.10	8.35	2.63	—	—	Flame + Ψ_{CE}		
AD	Axial	Oval	9.90	8.20	5.20	2.85	1.66	1.60	Flame		
AE	Axial	Oval	11.25	9.20	7.24	2.84	1.645	1.67	Flame		
AF	Axial	Near-round	7.24	7.00	2.60	2.80	1.64	1.59	Flame + Ψ_{CE}		
AG	Axial	Oval	9.00	7.55	4.04	2.84	1.64	1.58	n.d.	n.d.	n.d.
AH	Axial	Drop	10.21	9.62	7.11	2.81	1.64	1.59	Flame		n.d.
AI	Axial	Drop	12.20	8.40	6.61	2.81	1.63	1.58	Flame + Ψ_{CE}		
AJ	Axial	Bullet	7.52	14.46	5.58	2.82	1.61	1.58	Flame + Ψ_{CE}		
AK	Axial	Pear	7.98	6.78	2.72	2.82	1.655	1.60	Flame		n.d.
AL	Axial	Button	8.16	9.43	5.31	2.82	1.60	1.56	Flame		
AM	Axial	Oval	11.72	7.24	4.59	2.81	1.65	1.56	Flame		
AN	Axial	Oval	11.95	8.98	7.09	2.79	1.65	1.63	Flame		n.d.
AO	Axial	Spindle	17.59	9.33	10.67	2.79	1.64	1.59	Flame + Ψ_{CE}		
AP	Axial	Button	8.37	9.21	4.76	2.70	1.65	1.59	Flame		n.d.
AQ	Axial	Near-round	11.32	12.05	11.96	2.84	1.64	1.60	Flame		
AR	Axial	Oval	8.75	6.80	2.63	2.31	1.65	1.60	Flame		
AS	Axial	Pear	9.56	7.73	3.78	2.70	1.64	1.56	Flame + Ψ_{CE}		n.d.
AT	Axial	Pear	7.42	6.52	1.90	2.53	1.65	1.56	Flame	n.d.	
AU	Axial	Drop	10.06	5.17	1.83	2.62	1.63	1.62	Flame		
AV	Axial	Bullet	8.69	6.55	2.75	2.76	1.65	1.57	Flame		n.d.
AW	Axial	Bullet	7.69	6.11	2.10	2.82	1.64	1.58	Flame		
AX	Axial	Oval	10.11	7.7	3.79	2.81	1.63	1.60	Flame		
AY	Axial	Bullet	10.81	6.85	3.39	2.80	1.65	1.61	Flame	n.d.	n.d.
AZ	Axial	Oval	12.73	8.70	7.77	2.77	1.63	1.63	Flame		
BA	Axial	Oval	14.31	7.88	7.37	2.82	1.65	1.57	Flame	n.d.	n.d.
BB	Axial	Oval	9.16	6.85	3.38	2.79	1.62	1.63	Flame		n.d.
BC	Axial	Pear	9.00	9.10	4.20	2.77	1.64	1.61	Flame		n.d.
BD	Axial	Spindle	17.76	5.25	3.11	2.82	1.64	—	Flame + Ψ_{CE}		n.d.
BE	Axial	Bullet	9.53	5.94	2.53	2.80	1.64	1.57	Flame		n.d.
BF	Axial	Spindle	15.42	5.08	2.88	2.82	1.64	—	Flame		n.d.
BG	Axial	Spindle	13.60	5.70	3.24	2.81	1.65	—	Flame		
BH	Axial	Spindle	13.46	5.50	3.04	2.81	1.64	—	Flame	n.d.	n.d.
BI	None	Baroque	L = 14.42 W = 12.25 H = 8.71		9.40	2.78	1.64	—	n.d.	n.d.	n.d.
BJ	Axial	Spindle	12.33	0.30	1.67	2.76	1.64	—	Flame + Ψ_{CE}	n.d.	n.d.
BK	None	Baroque	L = 22.44 W = 13.45 H = 8.92		20.28	2.86	1.64	—	n.d.	n.d.	n.d.

^a Ψ_{CE} = pseudo-cat's-eye

^bThe two last columns indicate the direction of spirals or blade impellers described in the "Optical Features" section.

^cn.d. = not detected

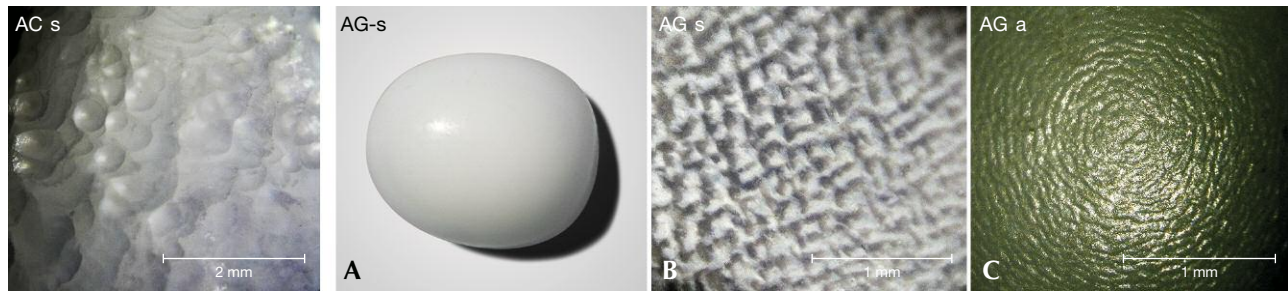


Figure 4. The photo on the far left reveals the texture of concave areas on flame-structure pearl AC. Pearl AG shows a satin-like appearance (A) and an orange peel structure along one side (B) and at the apex (C). Photos by J.-P. Gauthier.

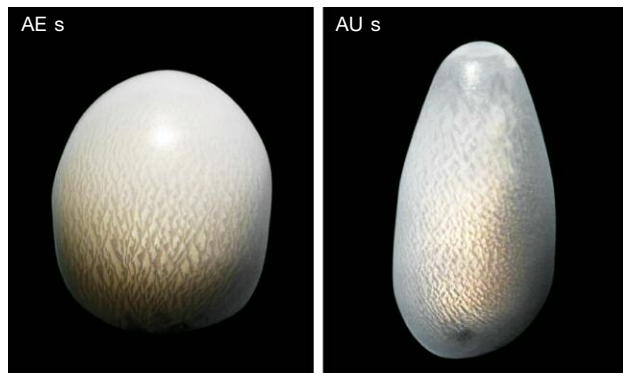
OPTICAL FEATURES

By far the most distinctive optical feature of the Tridacnidae samples was their flame structure. Some of the samples simply showed porcelaneous surfaces or appeared rather dull.

Surface Texture. At first, the brilliant surfaces of the flame-structure pearls appeared smooth. With low-angle lighting, however, one could observe numerous small, joined depressions (far left in figure 4, pearl AC). Most of the pearls had a high luster and displayed a porcelaneous sheen. Some pearls lacking flames (AG, BI, and BK) had a satin luster (figure 4A, pearl AG); at higher magnification, they presented an orange peel texture (figure 4B), axially centered in circles at the poles (figure 4C). No evidence of polishing or peeling (Strack, 2006) on the surface was found.

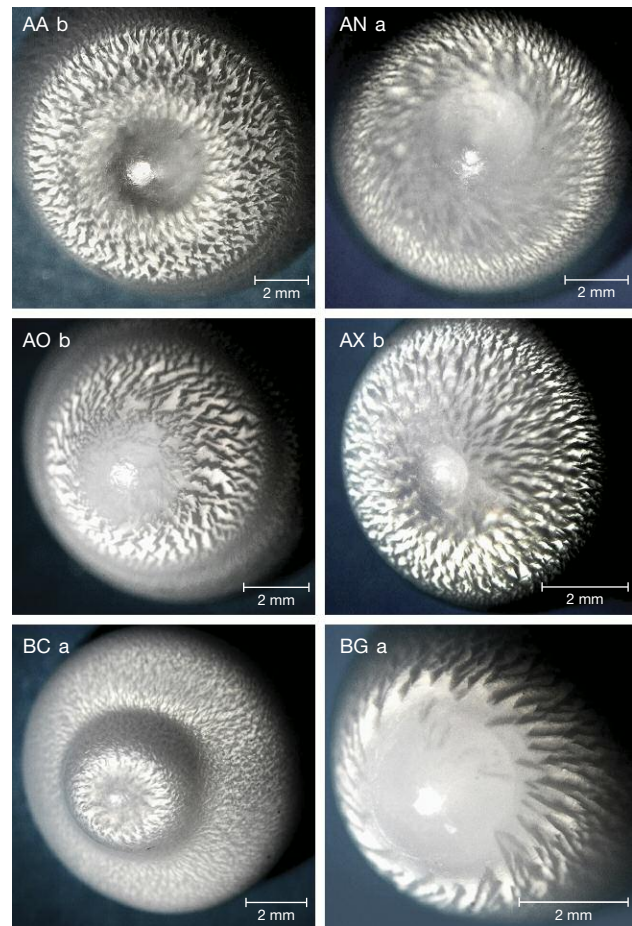
Flames. Lateral observation revealed a flame structure fanning out in one main direction, in a bright helix, around the rotation axis. The winding helices displayed a characteristic crisscross pattern (figure 5, pearls AE and AU). These helicoidal lines converged

Figure 5. Lateral observation of samples AE (left) and AU (right) shows a crisscross flame structure. Photos by J.-P. Gauthier.



toward the poles, resulting in dramatic patterns (figure 6). Moreover, a top view showed a non-radial convergence to the poles that resembled the structure of blade impellers oriented in the same direction and confirming the existence of a rotation axis (see figure 12).

Figure 6. Flame patterns observed at the apex or base of six pearls from the Tridacnidae family. Photos by J.-P. Gauthier.



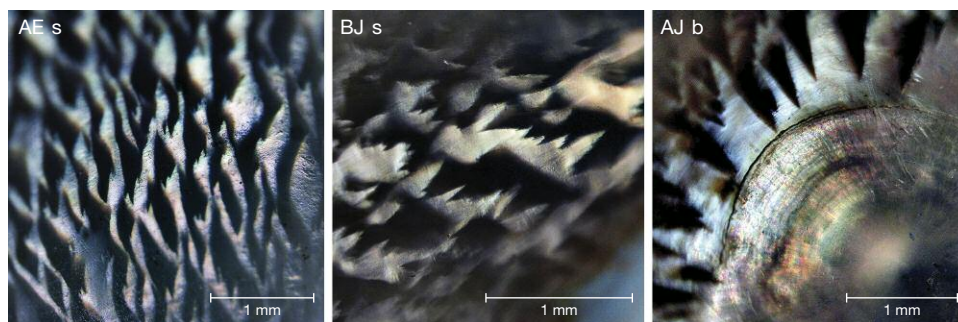


Figure 7. Left and center: These images of pearls AE and BJ show the directional growth of flames. Right: In pearl AJ, flames start from a pole with a two-dimensional spiral. Photos by J.-P. Gauthier.

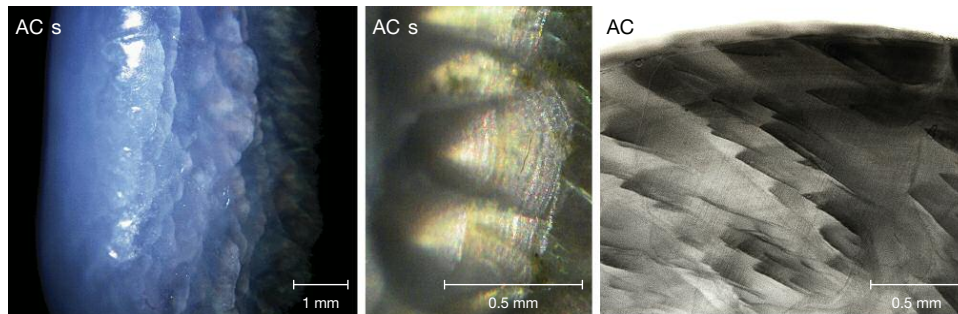


Figure 8. Left and center: Overlapping layers merging at the surface of pearl AC and their lamellar iridescent structure. Right: A thick slice cut perpendicular to the rotational axis of pearl AC shows the flames inclined with respect to the surface. Photos by J.-P. Gauthier.

In their finer structure, the shape and positions of the flames are more difficult to grasp, as their appearance changes depending on the light exposure. The term “flame” is justified by a wide base and a pointed tip, all oriented in the growth direction (figure 7, pearls AE and BJ). Alternating bright and dark areas are noted by Hänni (2010), while the cross-lamellar structure observed in conch pearls and shells is reminiscent of a previous study on the fracture toughness of the *Strombus gigas* shell (Kamat et al., 2000). Binocular microscopy allows us to better appreciate the three-dimensional configuration of the flames, which are less visible in

two-dimensional photographs. Through this process, we came to understand that these flames are not totally localized on the surface, but rather come from inside the pearl. This is confirmed by a photograph of a slice cut perpendicular to the rotation axis of pearl AC, as illustrated in figure 8 (right).

In some cases, the reflective parts instead have a scale-like shape (figure 8, left) perpendicular to the rotation axis. We then observe a pseudo-chatoyancy, shifted to the right or the left of the axis (figure 9, pearls AI and BD). The origin of this effect will be discussed later. It is also worth noting the helicoidal

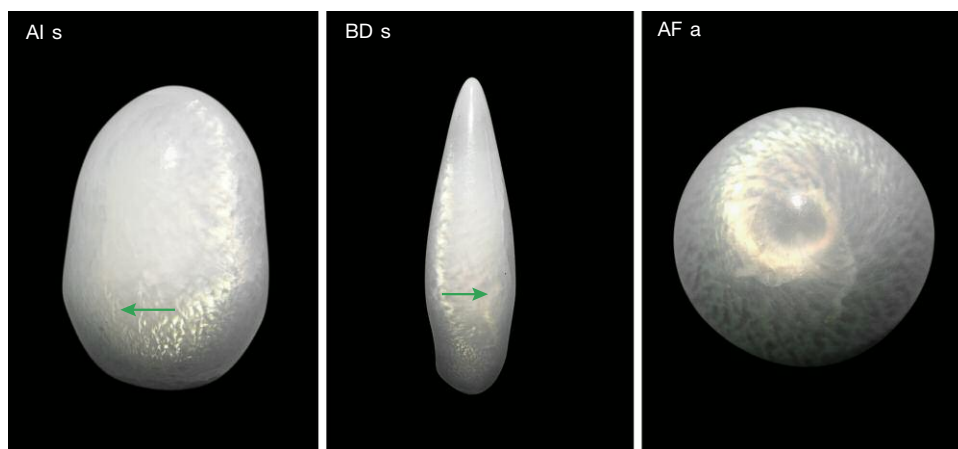


Figure 9. Pseudo-chatoyancy in pearls AI (left) and BD (center) and a helical effect in pearl AF (right). The bright spots in pearls AI and AF and the shiny median line close to the apex of pearl BD correspond to specular reflection. Green arrows represent the direction of rotation (according to figure 17). Photos by J.-P. Gauthier.

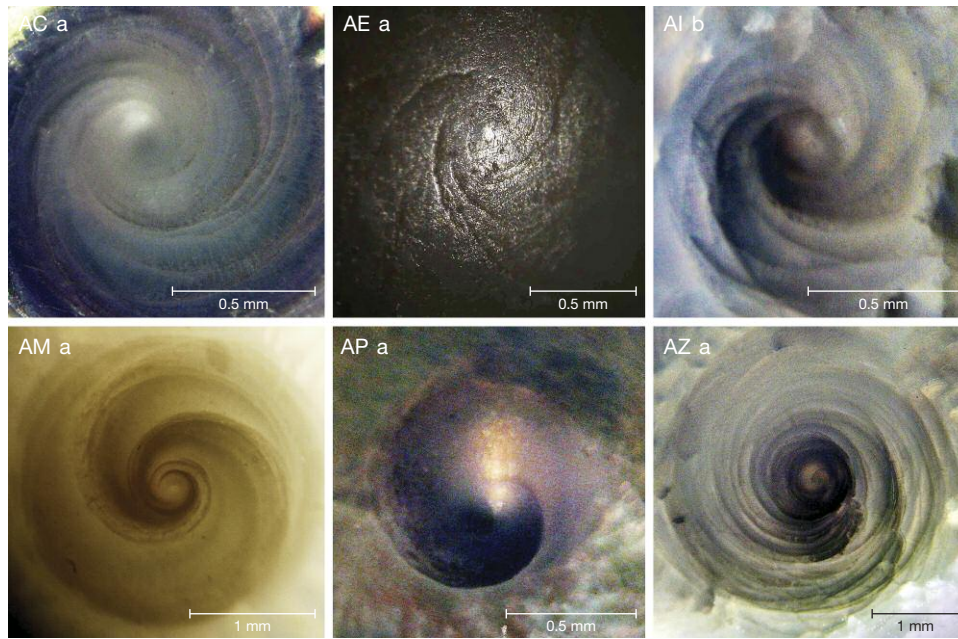


Figure 10. Three-dimensional spirals (or helices) merging at the poles of some *Tridacnidae* pearls. The images are processed using a high-pass filter. Photos by J.-P. Gauthier.

cat's-eye effect, visible in some samples but especially in pearl AF (figure 9, right).

The scales on the lateral part of the pearl (figure 8, left), which developed in laminated layering, are similar to nacre in their optical effect (interference and diffraction colors; see figure 8, center), as observed on the polished outer surface of *Pinctada margaritifera* shells (see figure 1 in Liu et al., 1999).

MAJOR OBSERVATIONS

Spirals. One of the most astounding characteristics found in some of the pearls is the spiral observed at the apex or base. This characteristic appears to be absent from the literature. Due to the difficulty of microscopic observation of the smooth white pearls, it was necessary to process the images and enhance the outlines by using a high-pass filter and forcing the contrast. Having gathered a number of images of these spirals, we determined that they fell into two types:

- The first has sharp outlines, often constituted by several branches, unfolding from the pole axis. Given the pearls' translucency, an internal helical structure seems to be emerging toward the surface. However, they exhibit no particular optical feature (figure 10).
- The second type has more tenuous outlines and presents only one branch at first glance. These spirals are flat and formed by radial crystallites in angular sectors of only a few degrees. Interference colors reveal that these spirals develop in thin layers. Examination at higher magnification also reveals narrow areas parallel to the edge of each spiral, constituting growth steps of low height (figure 11). In the case of pearl AI, the spiral is highlighted by air bubbles in water. This defines a local depression on the apex surface suitable for the deposition of these bubbles rather than for a smooth surface.

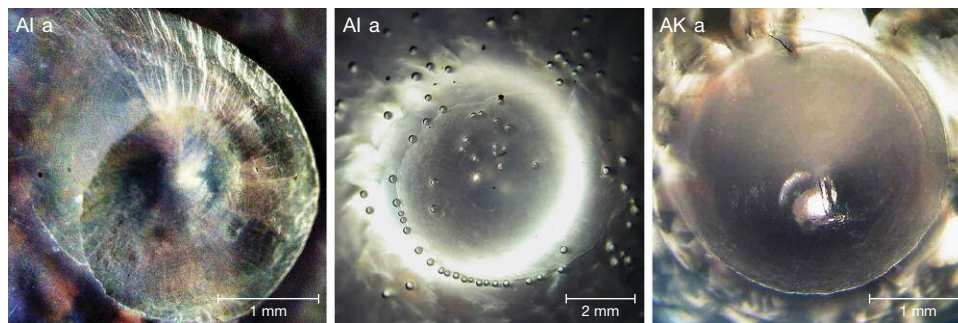


Figure 11. Two-dimensional spirals with radial sectors at the poles of some *Tridacnidae* pearls. The spiral of immersed pearl AI is highlighted by air bubbles in the depression on the surface. The images are processed using a high-pass filter. Photos by J.-P. Gauthier.

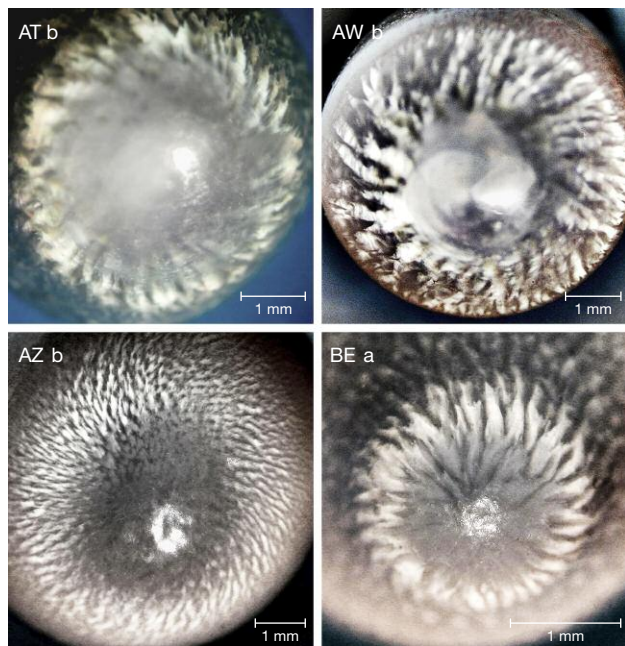


Figure 12. Some flame structures display a pattern at the poles that is reminiscent of blade impellers. Photos by J.-P. Gauthier.

Unfortunately, most of the spirals were barely visible and only a few were correctly identified, which made it impossible to evaluate statistics on their effective presence on one or both poles. In addition, these two types of spirals are likely to superimpose on each other. Note that the two types of spirals can be left- or right-handed.

Blade Impellers. At either the apex or the base, the flames often formed attractive patterns reminiscent of blade impellers or fan blades. These blades were all curved in one direction on a given pearl. Figure 12 shows typical examples.

Spirals and blade impellers, when present, do not always coexist. For an overview of the whole sample

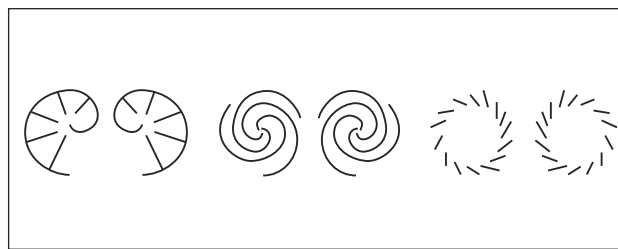


Figure 13. Clockwise and counterclockwise line drawings of two- and three-dimensional spirals (first four drawings from the left) and blade impellers (last two drawings on the right).

set of pearls, see table 1, which includes the rotation direction of spirals and blades for the apex as well as the base. The multiple branches of spirals represent the internal helices. The surface spirals have a single branch in addition to centripetal rays, suggesting angular growth sectors. A corona-shaped representation with directional blades is adopted for both the clockwise and counterclockwise blade impellers. The basic patterns are represented in figure 13. Depending on the orientation of the spirals and blade impellers, they can be used individually or combined. Figure 14 displays the superimposition of spirals and blade impellers, oriented in the same direction (left, pearl AN) or the opposite direction (right, pearl AE).

OTHER OBSERVATIONS

Defects. Four pearls (AC, AJ, AR, and BC) presented a surface defect visible to the eye (figure 15). These were related to a spot defect that extended into a depressed groove with a light yellowish hue, possibly consisting of organic material. Two of the four spot defects formed a depression and exhibited a chimney-like hole (pearls AC and AR).

Uncommon Features. Three pearls (AA, AB, and AO) presented a sharp and relatively thin circle perpendi-

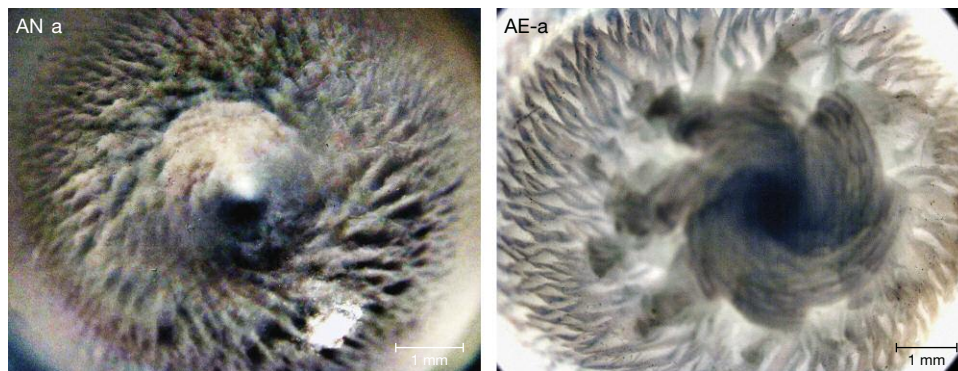


Figure 14. The flame structure at the apex, similar to blade impellers; the internal spiral shows a common (pearl AN) or opposite (pearl AE) direction. Photos by J.-P. Gauthier.

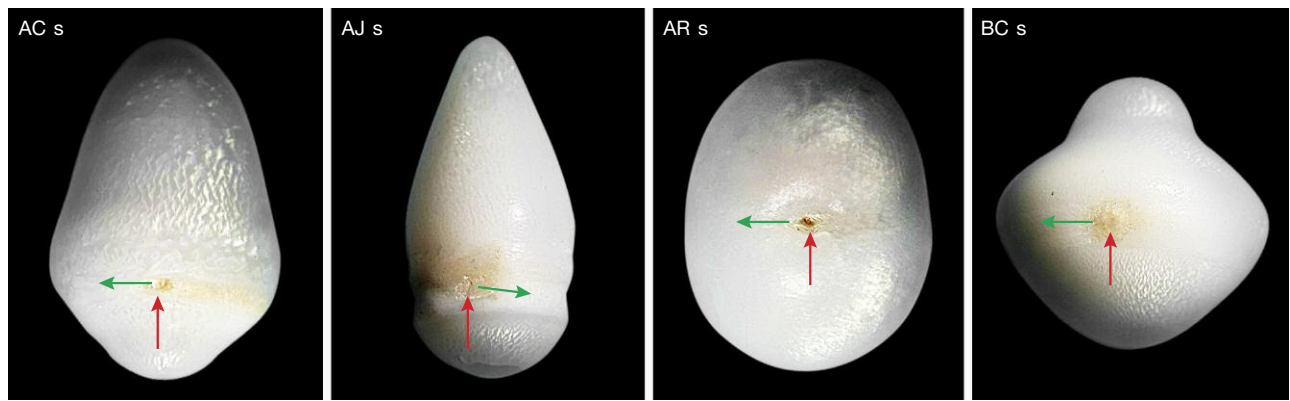


Figure 15. Spot defects observed on *Tridacnidae* pearls (red arrows) are accompanied by a comet, which indicates the direction of rotation (green arrows). Photos by J.-P. Gauthier.

cular to the rotation axis. These were not related to the circles observed in barrel-shaped pearls from *Pinctada* that are associated with spot defects (Gauthier et al., 2014). Rather, the circles revealed a separation line on the surface, characterized by a discontinuity of the flame growth direction (figure 16). Their origin remains unclear.

Translucency of Poles. In some cases, the flames did not cover the apex or the base. The light penetrated inside the pearl when the poles were illuminated in the direction of the rotation axis and was therefore not reflected by the flames. Subsequently the light was stopped by the lateral flames, which appeared dark (see figure 6, pearl BG). This translucency allowed for the observation of three-dimensionality in one spiral type, as described above.

DISCUSSION

Routine analyses confirmed the aragonitic nature of these pearls. They are exclusively white in color and do not fluoresce under UV light. While the exact origin of these pearls remains unknown, the variations

observed in the visual features could be linked to differences between *Tridacna* and *Hippopus* species. This hypothesis requires confirmation based on samples from known species and their respective shells, but such an analysis is outside the scope of the present study.

Several elements support the probability of pearl rotation during the growth phase:

Axial Symmetry. Among the set of 37 pearls, 35 exhibited cylindrical symmetry (see figure 2 and table 1). The pearls, which developed in the mantle tissue of the mollusk, did not grow around spherical nuclei and were not confined to limited spaces (as opposed to those cultivated in the gonads of saltwater oysters). Therefore, we must examine the rotation of these pearls to explain this symmetry. The rotation around a fixed axis takes place when the pearl settles in the mantle on anchorage points, specifically due to its nonspherical shape (Gauthier et al., 2014). Incidentally, the circle surrounding the three pearls in figure 16, perpendicular to their rotation axis, supports the likelihood of rotation.

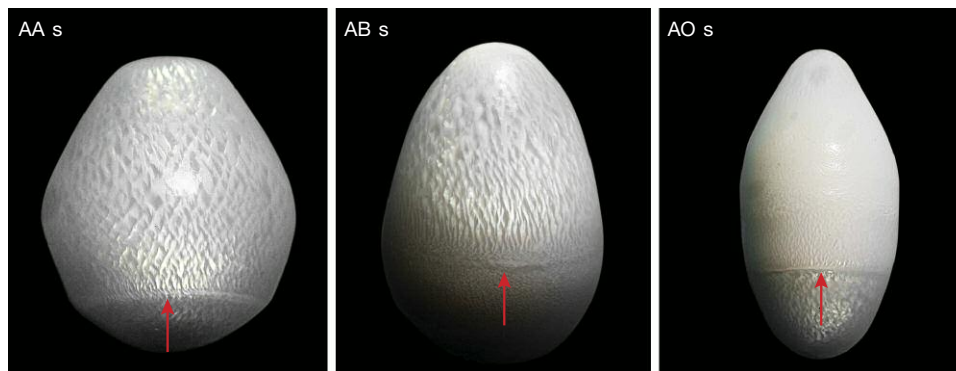


Figure 16. Circles observed at the bases of some pearls from *Tridacnidae*. Photos by J.-P. Gauthier.

Presence of Spirals at the Poles. As mentioned earlier, the spirals fell into two types. One was a three-dimensional spiral, most probably with internal helices from a genetic origin and possibly not related to rotation (see figure 10). The second type, a quasi-two-dimensional flat spiral of mechanical origin, was due to the deposition of aragonite at the poles, which grew in small angular sectors (see figure 11). The direction of rotation was opposite to the direction of the spiral development, as is the case with pearls from *Pinctada margaritifera* (Gueguen et al., 2015).

Flame Growth and Blade Impellers. Flames often developed along a helix, sometimes a double helix, located on or near the pearl surface. When looking at a coil spring, whether left- or right-handed, nothing indicated the direction in which it would turn. However, the flame spikes of a helix were all oriented in the same growth direction. The name “blade impellers” refers to the flames being displayed in a pattern, centered on the pearl’s axis when it reaches the pole (see figure 12). Whether by lateral or vertical observation, the pearl normally rotated in the direction opposite to the aragonite growth (Cartwright et al., 2013).

Pseudo-Chatoyancy. Some flame-structure pearls presented a bright line rising along their axis of symmetry (see figure 9) that resembled a cat’s-eye effect. Unlike chatoyancy in cabochon-cut gems, this does not result from a lattice of parallel acicular inclusions diffusing the light (Wüthrich and Weibel, 1981), but is instead due to a series of reflective blades oriented in the same direction, on or near the pearl surface (see figure 8, left and center). The pseudo-chatoyancy is produced by the reflection from this scale-like structure.

Observing the line of pseudo-chatoyancy is crucial to infer the direction of rotation. When both the light source and the observer are positioned upright over the pearl axis, which is horizontal, the bright line should be symmetrical if the blades lie on the surface (see the light path shown in red in figure 17). However, the blades come from the inner pearl in successive layers, as shown in figure 8. Consequently, the bright line is not observed in the median plane. Rather, it is off-center (see the light path marked in black in figure 17 as well as the pseudo-cat’s-eye in figure 9, pearls AI and BD). The rotation should then occur in the direction opposite the blade growth, again according to the theory of Cartwright et al. (2013). They suggest a rotation mechanism due to fundamental forces, acting

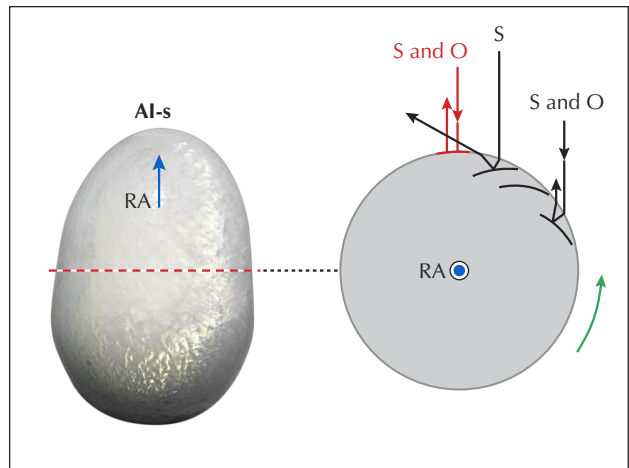


Figure 17. Left: As shown in figure 9, pearl AI displays a pseudo-chatoyancy. The red dashed line corresponds to the cross-section of the pearl, perpendicular to the rotational axis (RA) and represented in the sketch on the right. Right: Centered reflection on a hypothetical blade at the surface (in red), for light source (S) and observer (O) above the pearl. In fact, an off-center reflection on an inner pearl layer (in black) results in a pseudo-chatoyancy effect. The green arrow indicates the rotation derived from the position of the pseudo-cat’s-eye and the direction of scale-like growth. Photo by J.-P. Gauthier.

toward the growth steps of nacreous pearls. The findings regarding the layer-by-layer growth in pearls of *Pinctada margaritifera* (Gauthier et al., 2014) support this theory of rotation direction. Accordingly, in the blade configuration illustrated in figure 17, the rotation should be counterclockwise.

The direction of rotation suggested by the pseudo-cat’s-eye of pearls AI and BD (see figure 9) is consistent with the observation of the two-dimensional flat spiral at the apex (table 1). Additionally, the helical bright line related to the flames in figure 9 (pearl AF) is the consequence of pseudo-chatoyancy, which accounts for both the helical growth of flames and the pearl rotation.

Presence of Spot Defects. The spot defects located near the bases of four pearls (see figure 15) are accompanied by comets, defining the arc of the circles perpendicular to the rotation axis. As established with pearls from *Pinctada margaritifera* (Gauthier et al., 2014), these spot defects allow us to determine the direction of rotation, as shown by the green arrow.

The rotation direction of each pearl cannot be inferred from the figures due to their complexity. An unambiguous answer lies in less common but more

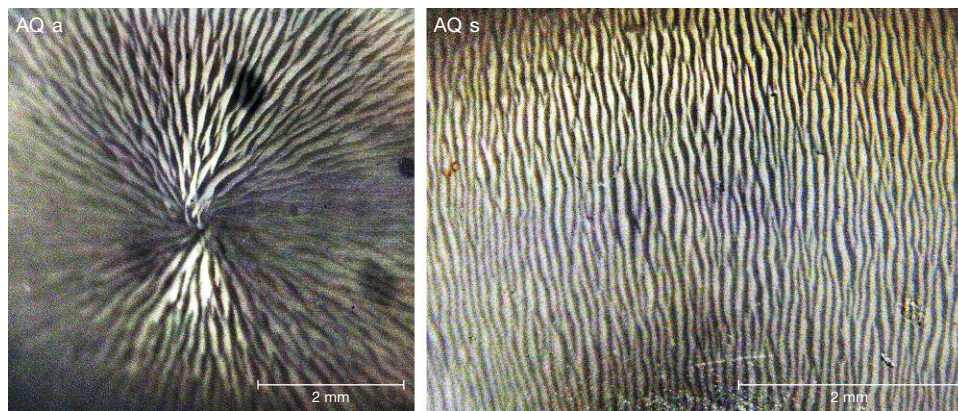


Figure 18. Observations of flame structures at the apex and equator of pearl AQ. Photos by J.-P. Gauthier.

reliable features, namely the two-dimensional spirals and comets associated with spot defects.

CONCLUSIONS

Besides the intrinsic gemological properties of flame-structure pearls from the Tridacnidae family, this study has stressed the predominance of axial symmetry, including unusual shapes unlike those generally encountered in nacreous pearls.

The two types of spirals, which have rarely been photographed, were often highlighted at the poles. The growth of flames produces some peculiar patterns on the pearls: blade impellers in the apex regions, pseudo-cat's-eyes on the sides, or circles resulting in caps at the two poles. Surface defects were identified, such as spot defects accompanied by comets. The axial symmetry, the directional growth of the flames, the pseudo-chatoyancy, the circles and

comets, and the blade impellers are all features that suggest the rotation of these pearls—if not during their formation, then at least during the growth phase preceding their harvest.

The unknown species origin of each Tridacnidae pearl leaves open the reasons for the observed visual differences, for example in the polar and equatorial flame patterns on pearl AQ (figure 18). Investigation of the internal structure definition, probably constituted of internal helices, will require the sacrifice of some pearls through cuts made parallel and perpendicular to the rotation axis.

It would also be interesting to investigate the flame-structure concretions of gastropods, such as conch “pearls,” that show evidence of rotation. However, these pearls rarely present an axial symmetry, and their scarcity is a major obstacle to the systematic study of this property.

ABOUT THE AUTHORS

Dr. Gauthier is a professor of physics retired from the University Claude Bernard Lyon I and now with the Gemological Research Center of Nantes (CRG) and the Association Française de Gemologie (AFG). Mr. Fereire is also a member of CRG and AFG. Mr. Bui is a civil engineer and researcher working at the Catholic University of Louvain in the field of nanophysics. He is a lecturer at HRD Antwerp and collaborates with that institute and the CRG on gemological research.

ACKNOWLEDGMENTS

This work was partially funded by Almini Beijing Trading Co. Ltd., China. The authors thank Erwann Jeanneau and Ruben Vera, from the Centre de Diffractométrie Henri Longchambon (Claude Bernard University Lyon I), for the X-ray analysis. They express their sincere gratitude to Tommy Bui for proofreading the English text.

REFERENCES

- Acosta-Salmón H., Davis M. (2007) Inducing relaxation in the queen conch *Strombus gigas* (L.) for cultured pearl production. *Aquaculture*, Vol. 262, No. 1, pp. 73–77, <http://dx.doi.org/10.1016/j.aquaculture.2006.09.032>
- Agbaje O.B.A., Wirth R., Morales L.F.G., Shirai K., Kosnik M., Watanabe T., Jacob D.E. (2017) Architecture of crossed-lamellar bivalve shells: the southern giant clam (*Tridacna derasa*, Röding, 1798). *Royal Society Open Science*, Vol. 4, No. 9, 170622, <http://dx.doi.org/10.1098/rsos.170622>
- Bari H., Lam D. (2009) *Perles*. Skira Ed., Milan, 335 pp.
- Bidwell D., DelRe N., Widemann A., Epelboym M. (2011) Natural non-nacreous pearls from the giant clam *Tridacna gigas*. *Ge@G*,

- Vol. 47, No. 2, pp. 144–145.
- Cartwright J.H.E., Checa A.G., Rousseau M. (2013) Pearls are self-organized natural ratchets. *Langmuir*, Vol. 29, No. 26, pp. 8370–8376, <http://dx.doi.org/10.1021/la4014202>
- Chang J.W., Hyatt A. (2011) Lab Notes: Large conch pearl. *G&G*, Vol. 47, No. 3, pp. 230–231.
- Copland J.W., Lucas J.S. (1988) *Giant Clams in Asia and the Pacific*. ACIAR Monograph No. 9, 274 pp.
- Council of the European Union (1997) Council Regulation (EC) No 338/97 of 9 December 1996 on the protection of species of wild fauna and flora by regulating trade therein. *Official Journal of the European Communities*, L61, Vol. 40, p. 60.
- Dauphin Y., Denis A. (2000) Structure and composition of the aragonitic crossed lamellar layers in six species of Bivalvia and Gastropoda. *Comparative Biochemistry and Physiology Part A*, Vol. 126, No. 3, pp. 367–377, [http://dx.doi.org/10.1016/S1095-6433\(00\)00213-0](http://dx.doi.org/10.1016/S1095-6433(00)00213-0)
- Davis M. (2000) Queen conch (*Strombus gigas*) culture techniques for research, stock enhancement and growout markets. In M. Fingerman and R. Nagabhushanam, Eds., *Recent Advances in Marine Biotechnology, Volume 4: Aquaculture, Part A: Seaweeds and Invertebrates*. Science Publishers, Inc., Enfield, New Hampshire, pp. 27–59, and other references in this chapter.
- Davis M., Shawl A.L. (2005) A guide for culturing queen conch. In A.M. Kelly and J.T. Silverstein, Eds., *Aquaculture in the 21st Century: Proceedings of an American Fisheries Society Symposium Special Symposium on Aquaculture in the 21st Century*, August 22, 2001, Phoenix, Arizona, pp. 125–142. American Fisheries Society, Bethesda, Maryland.
- Federman D., Bari H. (2007) *La perle rose: trésor naturel des Caraïbes*. Skira Ed., Milan, 176 pp.
- Fritsch E., Misirowski E.B. (1987) The history and gemology of queen conch “pearls.” *G&G*, Vol. 23, No. 4, pp. 208–221, <http://dx.doi.org/10.5741/gems.23.4.208>
- Gannon M.E., Pérez-Huerta A., Aharon P., Street S.C. (2017) A biomineralization study of the Indo-Pacific giant clam *Tridacna gigas*. *Coral Reefs*, Vol. 36, No. 2, pp. 503–517, <http://dx.doi.org/10.1007/s00338-016-1538-5>
- Garen P. (2003) Ponte et élevage larvaire de bénitier (*Tridacna maxima*). IFREMER, Note technique, 5 pp.
- Gauthier J.-P., Gutierrez G., Serrar M. (2014) La “piqûre”, un défaut à l’origine du cerclage de perles chez *Pinctada margaritifera*. *Revue de Gemmologie a.f.g.*, No. 187, pp. 4–6.
- Gauthier J.-P., Gutierrez G., Serrar M., Bui T.N. (2015) Rares perles cerclées à double axe de rotation. *Revue de Gemmologie a.f.g.*, No. 194, pp. 4–7.
- Gauthier J.-P., Fereire J., Bui T.N. (2018) An explanation of a specific type of circling as observed on Ming cultured pearls. *Journal of Gemmology*, Vol. 36, No. 3, pp. 152–160, <http://doi.org/10.15506/jog.2018.36.3.240>
- Gueguen Y., Czorlich Y., Mastail M., Le Tohic B., Defay D., Lyonard P., Marigliano D., Gauthier J.-P., Bari H., Lo C., Chabrier S., Le Moullac G. (2015) Yes, it turns: experimental evidence of pearl rotation during its formation. *Royal Society Open Science*, Vol. 2, No. 7, p. 150144, <http://dx.doi.org/10.1098/rsos.150144>
- Hänni H.A. (2010) Explaining the flame structure of non-nacreous pearls. *Australian Gemmologist*, Vol. 24, No. 4, pp. 85–88.
- Ho J.W.Y., Zhou C. (2014) Lab Notes: Natural pearls reportedly from a *Spondylus* species (“thorny” oyster). *G&G*, Vol. 50, No. 3, pp. 241–242.
- Homkrajac A. (2016a) Micro-World: Iridescent *Spondylus* pearl. *G&G*, Vol. 52, No. 2, pp. 202–203.
- (2016b) Lab Notes: Non-nacreous purple and white pearls reportedly from *Spondylus* species. *G&G*, Vol. 52, No. 3, pp. 303–304.
- Htun H., Larson W., Cole J.E. (2006) Melo “pearls” from Myanmar. *G&G*, Vol. 42, No. 3, pp. 135–136.
- Hui M. (2012) Connectivity and evolution of giant clams (Tridacnidae): A molecular genetic approach. PhD thesis, University of Bremen, 85 pp.
- Hyatt A. (2008) Lab Notes: Large baroque multicolored conch pearl. *G&G*, Vol. 44, No. 1, p. 72.
- Jiao D., Liu Z.Q., Qu R.T., Zhang Z.F. (2016) Anisotropic mechanical behaviors and their structural dependences of crossed-lamellar structure in a bivalve shell. *Materials Science and Engineering C*, Vol. 59, pp. 828–837, <http://dx.doi.org/10.1016/j.msec.2015.11.003>
- Kamat S., Su X., Ballarini R., Heuer A.H. (2000) Structural basis for the fracture toughness of the shell of the conch *Strombus gigas*. *Nature*, Vol. 405, No. 6790, pp. 1036–1040, <http://dx.doi.org/10.1038/35016535>
- Koivula J.I., Kammerling R.C., Fritsch E. (1994) Gem News: Horse conch “pearls.” *G&G*, Vol. 30, No. 3, p. 195.
- Liu Y., Shigley J.E., Hurwit K.N. (1999) Iridescence color of a shell of the mollusk *Pinctada margaritifera* caused by diffraction. *Optics Express*, Vol. 4, No. 5, pp. 177–182, <http://dx.doi.org/10.1364/OE.4.000177>
- Scarratt K. (1999) Orange pearls from the Melo volutes (marine gastropods). In D.J. Content, Ed., *The Pearl and the Dragon: A Study of Vietnamese Pearls and a History of the Oriental Pearl Trade*. Rare Books Incorporated, Houlton, Maine, pp. 80–107.
- Segura O., Fritsch E. (2015) Gem News International: Nonbead-cultured pearls from *Strombus gigas*. *G&G*, Vol. 51, No. 2, pp. 201–202.
- Singbamroong S., Ahmed N., Ahmed A.R., Karam M., Hassan G., Mohamed S., Al Muhairi N. (2015) Observations on natural non-nacreous pearls reportedly from *Tridacna* (clam) species. *34th International Gemmological Conference IGC*, pp. 125–127.
- Strack E. (2006) *Pearls*. Rühle-Diebener-Verlag, Stuttgart, Germany, 707 pp.
- Wüthrich A., Weibel M. (1981) Optical theory of asterism. *Physics and Chemistry of Minerals*, Vol. 7, No. 1, pp. 53–54, <http://dx.doi.org/10.1007/BF00308202>